

Relating Organic Fouling of Reverse Osmosis Membranes to Intermolecular Adhesion Forces

SANGYOUP LEE AND
MENACHEM ELIMELECH*

Department of Chemical Engineering, Environmental Engineering Program, Yale University, New Haven, Connecticut 06520-8286

Organic fouling of reverse osmosis (RO) membranes and its relation to foulant–foulant intermolecular adhesion forces has been investigated. Alginate and Suwannee River natural organic matter were used as model organic foulants. Atomic force microscopy was utilized to determine the adhesion force between bulk organic foulants and foulants deposited on the membrane surface under various solution chemistries. The measured adhesion force was related to the RO fouling rate determined from fouling experiments under solution chemistries similar to those used in the AFM measurements. A remarkable correlation was obtained between the measured adhesion force and the fouling rate under the solution chemistries investigated. Fouling was more severe at solution chemistries that resulted in larger adhesion forces, namely, lower pH, higher ionic strength, presence of calcium ions (but not magnesium ions), and higher mass ratio of alginate to Suwannee River natural organic matter. The significant adhesion force measured with alginate in the presence of calcium ions indicated the formation of a crossed-linked alginate gel layer during fouling through intermolecular bridging among alginate molecules.

Introduction

Reverse osmosis (RO) membranes are presently being used in a wide range of applications, including brackish/seawater desalination, drinking water treatment, and wastewater reclamation. Of particular interest is the use of RO membranes in advanced wastewater reclamation to augment limited available water supply. Efficient application of RO membrane technology in wastewater reclamation is significantly hampered by the phenomenon of organic fouling as wastewater effluent contains a considerable amount of organic substances (1, 2), designated as effluent organic matter. Fouling results in reduced water flux and compromised permeate quality. Therefore, understanding the mechanisms governing organic fouling is of paramount practical importance for sustainable application of RO membrane technology.

The formation of a fouling layer on the membrane surface—referred to as surface fouling—is the dominant fouling mechanism for RO because RO membranes are considered “nonporous”. Surface fouling involves the initial deposition of organic foulants on the membrane surface and the subsequent growth of a fouling layer that adversely

influences membrane performance. Initial foulant deposition on the membrane surface is controlled by the interaction between the bulk foulants and the membrane surface. Intermolecular adhesion between the bulk foulants and the foulants deposited on the membrane surface primarily controls the evolution of the fouling layer. For most practical applications, the rate and extent of organic fouling are determined by the foulant–foulant interactions because monolayer coverage on the membrane surface through foulant–membrane interactions is attained in a very short period of time (3). Foulant–foulant interactions are also responsible for the fouling layer structure (thickness and compactness), which determines the hydraulic resistance of the fouling layer and, thus, the flux–decline behavior during fouling (4). Hence, quantification of foulant–foulant adhesion can provide molecular-level understanding of the mechanisms governing organic fouling.

Atomic force microscopy (AFM) allows the measurement of a variety of interaction forces in aqueous solutions (5, 6). AFM force measurements have recently been applied to membrane research (7–9). Measurements of interaction forces between a colloid probe and a membrane surface enable quantification of the electrostatic double layer interaction when the colloid probe approaches the membrane surface, and of the adhesion force when the colloid probe is retracted after it has been in contact with the membrane surface. Therefore, foulant–foulant adhesion can be quantified from the force versus separation distance curves determined during the retraction of the foulant probe from the fouled membrane surface. In addition, the influence of solution chemistry (pH, ionic strength, and divalent cations) on foulant–foulant adhesion can be assessed by varying the ionic composition of the test solutions during force measurements.

Studies on the use of AFM to measure the interaction forces governing membrane fouling are rather scarce. Li and Elimelech (3) were first to demonstrate that the intermolecular adhesion force between bulk humic acid and humic acid deposited on the membrane surface controls the rate of humic acid fouling of nanofiltration membranes. To date, however, no direct relationship between foulant–foulant adhesion and organic fouling behavior of RO membranes under various solution chemistries has been reported.

In this study, AFM, in conjunction with a particle/foulant probe, was used to quantify the intermolecular adhesion force between the bulk foulants and the foulant deposited on the membrane surface. Fouling experiments were performed under solution chemistries similar to those employed in the AFM force measurements to allow direct comparison of fouling rate to the foulant–foulant adhesion force. A remarkable correlation was obtained between the measured adhesion force and the membrane fouling rate under the solution chemistries investigated, suggesting AFM force measurement as a tool to predict membrane fouling potential.

Materials and Methods

Organic Foulants. Alginate and Suwannee River natural organic matter (SRNOM) were used as model organic foulants since acidic polysaccharides and, to a lesser extent, humic-like substances are the major components of effluent organic matter (1, 10–12). Alginate (Sigma-Aldrich, St. Louis, MO) and SRNOM (International Humic Substances Society, St. Paul, MN) were received in a powder form. Stock solutions (2 g/L) were prepared by dissolving the organic foulants in deionized (DI) water (with no pH adjustment), followed by

* Corresponding author phone: (203) 432 27890; fax (203) 432 2881; e-mail: menachem.elimelech@yale.edu.

filtration with a 0.45 μm filter (Millipore, Billerica, CA). The stock solutions were stored in sterilized glass bottles at 4 °C. Based on the manufacturer's specifications, the alginate was extracted from brown algae and the molecular weight (MW) ranges from 12 to 80 kDa. The humic content (i.e., hydrophobic acids adsorbed on XAD-8 resin (13)) and MW of the SRNOM have been reported to be 70–75% and 1500–2500 g/mole, respectively (14).

Charge density (carboxylic and/or phenolic acidity) of the model organic foulants was determined by potentiometric titration. The sample solution for titration contained 100 mg/L organic foulant and 10 mM NaCl as a background electrolyte. The solution was first acidified with 1.0 M HCl to pH 2.9 so that all of the carboxylic groups would become protonated. The pK_a values of the carboxylic acid of alginate (15) and humic acid (16) have been reported to be about 3.0 and 3.4, respectively, and are not significantly affected by the ionic strength. Following the pH adjustment, the sample solution was titrated to pH 10.0 with 0.1 M NaOH using an automatic titrator (794 Basic Titrino, Metrohm, Switzerland). During the titration, N_2 gas was introduced continuously into the titration vessel to maintain a carbonate-free atmosphere. The titration vessel was located on a magnetic stirrer to provide complete mixing of the sample solution upon addition of the NaOH during the titration. Blank titration was performed with a foulant-free 10 mM NaCl solution at the same conditions as those employed during the sample titration. The amount of NaOH added during the blank titration served to determine the net amount of NaOH consumed to deprotonate the carboxylic and/or phenolic functional groups of the organic foulants.

RO Membrane. The aromatic polyamide thin-film composite LFC-1 (Hydranautics, Oceanside, CA) was selected as a model RO membrane for the fouling experiments and AFM force measurements. This relatively well-characterized membrane has been widely used for brackish water desalination, wastewater reclamation, and drinking water treatment (17). The membrane has been reported to be negatively charged at solution chemistries typical of natural and waste waters, with an isoelectric point at about pH 4 (17). The hydraulic resistance was determined to be $9.16 (\pm 0.11) \times 10^{13} \text{ m}^{-1}$. The salt rejection was 98.7–99.3%, determined with a 10 mM NaCl solution, an applied pressure of 2.07 MPa (300 psi), and a cross-flow velocity of 8.56 cm/s.

Solution Chemistry. All chemicals were reagent grade and were used without further purification. ACS grade NaCl, $\text{MgCl}_2 \cdot 6\text{H}_2\text{O}$, and $\text{CaCl}_2 \cdot 2\text{H}_2\text{O}$ salts, as well as trace metal HCl and NaOH, were obtained from Fisher (Pittsburgh, PA). Stock solutions were prepared fresh using DI water.

Solution chemistries investigated for both AFM force measurements and fouling experiments included variations in pH, indifferent electrolyte concentration (NaCl), divalent cations (Mg^{2+} and Ca^{2+}), and dissolved organic foulant composition. In all cases, identical solution chemistries were employed in both fouling experiments and AFM force measurements to allow direct comparison. The pH of the solution was adjusted to the desired value by adding 0.1 M HCl or NaOH stock solutions. When investigating the effect of divalent cation (Mg^{2+} or Ca^{2+}) concentration, the solution was amended to the desired value by adding 0.1 M $\text{MgCl}_2 \cdot 6\text{H}_2\text{O}$ or $\text{CaCl}_2 \cdot 2\text{H}_2\text{O}$ stock solutions, while the total ionic strength was maintained constant by adjusting NaCl concentration. The organic foulant composition was varied as needed by adjusting the ratio of the alginate to SRNOM concentration, while the total organic foulant concentration was kept constant.

Fouling Experiments. A laboratory-scale cross-flow membrane test unit, similar to that employed by Ang et al. (18), was used for the fouling experiments. The rectangular plate-and-frame cell has dimensions of 7.7-cm length, 2.6-cm

width, and 0.3-cm height. The system was operated in a closed-loop mode with both permeate and retentate being recirculated into the feedwater reservoir. Temperature was maintained constant during the fouling runs by a temperature controller with a stainless steel coil submerged in the feedwater reservoir. Permeate flux was recorded continuously by a digital flow meter interfaced with a PC.

Fouling experiments were performed at fixed hydrodynamic operating conditions, namely initial flux and cross-flow velocity. The protocol for all fouling experiments comprised these sequential steps. The membrane was first compacted with DI water in the membrane test cell for 12 h. Then, the membrane was stabilized and equilibrated for an additional 6 h with foulant-free electrolyte solution having solution chemistry identical to that used for the subsequent fouling run. After attaining a stable permeate flux, the initial flux and the cross-flow velocity were adjusted to 20 $\mu\text{m/s}$ and 8.56 cm/s, respectively, and the run continued for 2 more hours. Organic fouling was then initiated by adding an organic foulant stock solution to the feedwater to achieve a 20 mg/L concentration of organic foulant.

Intermolecular Adhesion Force Measurements and Analysis. Intermolecular adhesion force was measured using a Nanoscope III multimode AFM (Digital Instruments, Santa Barbara, CA). A carboxylate modified latex (CML) particle (Interfacial Dynamics Corp., Portland, OR) was used for making the AFM colloid probe because the model organic foulants used in this study (alginate and SRNOM) contain predominantly carboxylic functional groups. A fluid cell was used to allow force measurements at the desired solution chemistries, with the membrane being located on the bottom of the fluid cell.

The experimental protocol for measuring the foulant–foulant adhesion force was based on the method reported by Li and Elimelech (3). Briefly, the procedure involved the following steps: (i) making a colloid probe by gluing the CML particle (4 μm in diameter) to a commercial tipless SiN cantilever (Veeco Metrology Group, Santa Barbara, CA) having a spring constant of 0.06 N/m; (ii) locating the membrane on the AFM dither piezo drive using a disk, with the membrane surface being upward; (iii) installing the colloid probe inside the fluid cell, followed by mounting the fluid cell on the membrane with an O-ring placed between the two to prevent leakage; (iv) rinsing the fluid cell with DI water three times, followed by an additional three rinses with the test solution; (v) filling the fluid cell with the test solution containing organic foulants, followed by equilibrating the system for 60 min; and (vi) initiating the force measurements, with the colloidal probe being engaged in successive movements of approaching, and retracting from, the membrane surface. Data obtained during the retraction of the colloid probe from the membrane surface were used to determine the adhesion forces.

Force measurements were performed at five different locations on the membrane surface, with 10 measurements at each location to minimize inherent variability in the force data, which is also contributed to by local membrane surface heterogeneity. Averaged AFM raw data (i.e., cantilever deflection with respect to cantilever displacement) were used to produce a force versus separation distance curve. By inspecting the generated cantilever deflection versus displacement curves for each chemical condition, substantially different curves were excluded prior to the averaging. In the absence of multiple jump-off events (19) during the adhesion force measurements, all curves were quite similar and, hence, most of the AFM data were included in the averaging. However, when multiple jump-off events took place (notably for runs with Ca^{2+}), raw data obtained from the same location on the membrane were somewhat varied. In this case, several comparable data sets selected from different locations were

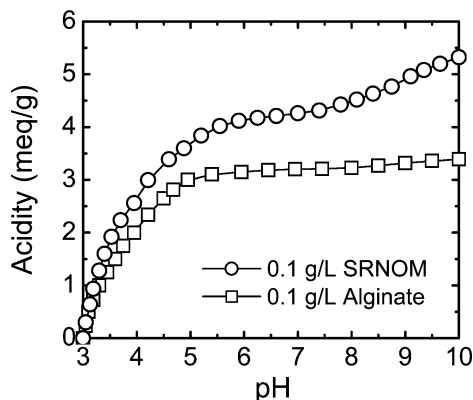


FIGURE 1. Acidity of alginate and SRNOM as a function of pH. Concentration of alginate and SRNOM is 0.1 g/L and test solution contains 10 mM NaCl as a background electrolyte. Potentiometric titration was performed from pH 3.0 to 10.0 with 0.10 M NaOH under a carbonate-free N_2 atmosphere at 23.0 ± 0.5 °C. Blank tests were carried out with foulant-free electrolyte solution (i.e., 10 mM NaCl) prior to each sample titration.

averaged. Finally, the averaged raw data of cantilever deflection with respect to cantilever displacement were converted to force–distance curves by the method reported by Ducker et al. (5, 20).

Derjaguin's approximation (21) states that the interaction force between a spherical particle and a planar surface is related to the interaction energy per unit area via

$$F(h) = 2\pi RW(h) \quad (1)$$

where $F(h)$ is the interaction force between the sphere and the flat surface separated by a distance h , R is the radius of the spherical particle, and $W(h)$ is the interaction energy per unit area between a sphere and a flat surface separated by a distance of h . According to eq 1, the interaction energy W is equal to F/R multiplied by a factor of 2π . Similarly, the adhesion force normalized by the radius of the particle and the flat surface by an infinite distance, $W(\infty)$ (3):

$$\frac{F_{ad}}{R} = 2\pi W(\infty) \quad (2)$$

F_{ad}/R can, therefore, be viewed as a measure of the energy required to prevent a foulant from accumulating on the membrane surface. For a given system, F_{ad}/R should be a good indicator of the membrane fouling potential. Consequently, all AFM force data in this study will be presented as the measured force normalized by the CML particle radius as a function of separation distance.

Results and Discussion

Charge Characteristics of Organic Foulants. Charge characteristics of organic foulants play an important role in fouling because electrostatic interactions between foulant molecules directly influence intermolecular adhesion. The acidity of alginate and SRNOM was determined by potentiometric titration and shown as a function of pH in Figure 1. Carboxylic and phenolic groups are the dominant functional groups of organic macromolecules in natural and waste waters (1, 22, 23). In practice, acidity up to pH 8.0 is attributed to the deprotonation of carboxylic groups, while above pH 8.0, it is attributed to phenolic groups (23). Figure 1 indicates that there was no further increase in the alginate acidity above pH 8.0, implying that carboxylic groups are the predominant

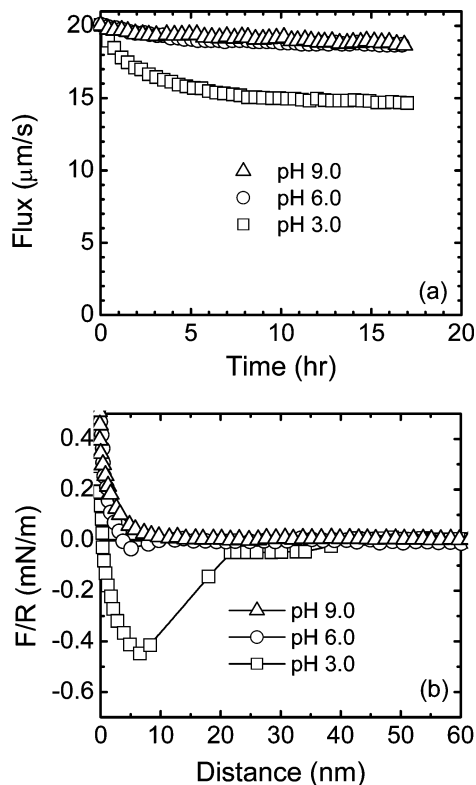


FIGURE 2. Effect of solution pH on (a) flux decline during fouling and (b) intermolecular adhesion force. Both fouling runs and force measurements were performed with identical solutions (i.e., alginate = 20 mg/L and ionic strength = 10 mM NaCl). The pH of the test solutions was adjusted by adding 0.1 M HCl or NaOH stock solutions. Experimental conditions during the fouling runs: initial flux = 20 $\mu\text{m/s}$, cross-flow velocity = 8.56 cm/s, and temperature = 20.0 ± 0.5 °C. Experimental conditions during the interfacial force measurements: equilibration time = 60 min and temperature = 23.0 ± 0.5 °C.

functional groups. In case of SRNOM, the increase in acidity above pH 8.0 is presumably due to the deprotonation of phenolic groups. The increase in the SRNOM acidity up to pH 8.0, however, is much more prominent than above pH 8.0. Thus, for both alginate and SRNOM, carboxylic functional groups are expected to control the electrostatic interactions between foulant molecules.

Influence of Solution pH. To investigate the influence of pH on alginate fouling, fouling experiments were performed with feed solutions at pH 3.0, 6.0, and 9.0. The flux–decline curves obtained during each fouling run are compared with the adhesion force curves determined by AFM in Figure 2. Test solutions containing 20 mg/L alginate and 10 mM NaCl were used in both fouling experiments and force measurements. A much lower flux decline was observed at pH 6.0 and 9.0 compared to pH 3.0. Similarly, substantial adhesion force (negative value of F/R) was observed at pH 3.0, whereas negligible adhesion force was detected at pH 6.0 and no adhesion at pH 9.0.

At pH 6.0 and 9.0, the carboxylic groups of alginate molecules in bulk solution and on the membrane surface were almost completely deprotonated, as implied from Figure 1, where the maximum acidity was already attained at pH 5.0. This leads to an increase in the electrostatic repulsion between alginate molecules, thus lessening intermolecular adhesion among alginate molecules. On the other hand, alginate molecules at pH 3.0 are uncharged, leading to an increase in alginate–alginate adhesion. The increase in intermolecular adhesion initiates the formation of an alginate fouling layer on the membrane surface, leading to more flux

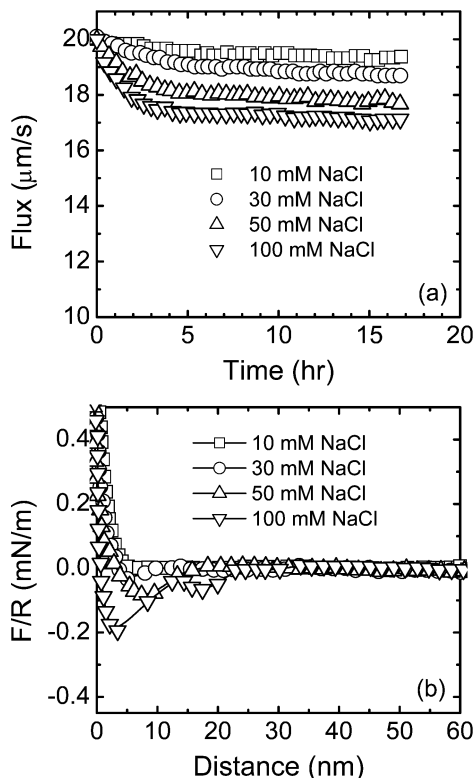


FIGURE 3. Effect of ionic strength on (a) flux decline during fouling and (b) intermolecular adhesion force. Both fouling runs and force measurements were performed with identical solutions (i.e., alginate = 20 mg/L and pH = 6.0 ± 0.1). The ionic strength of the test solutions was adjusted by varying indifferent salt (i.e., NaCl) concentration. Other experimental conditions during the fouling runs and the force measurements were identical to those in Figure 2.

decline. Similar trends of a more substantial flux decline with decreasing pH for charged organic macromolecules (humic acid, NOM, and proteins) were observed in other studies (4, 24, 25). The results shown here demonstrate that reduction in electrostatic interactions at low pH enhances foulant–foulant adhesion, which results in increased fouling.

Influence of Indifferent Electrolyte Concentration. The influence of ionic strength on the flux–decline behavior during alginate fouling and the corresponding intermolecular adhesion is presented in Figure 3. Solution chemistries for the force measurements were identical to the feed solution chemistries employed during the fouling experiments. It is clearly shown that flux decline as well as alginate adhesion became more substantial with increasing ionic strength. At higher ionic strengths, the electric double layer around charged alginate molecules is compressed, which reduces electrostatic repulsion between alginate molecules in bulk solution and on the membrane surface. This leads to an increase in the intermolecular adhesion between alginate molecules and, consequently, to a thicker and more compact fouling layer on the membrane surface. However, the maximum adhesion force determined at the highest ionic strength (i.e., 100 mM) is only -0.21 mN/m, less than half of the adhesion force measured at pH 3.0 (Figure 2b). Similarly, the flux decline at 100 mM ionic strength is less substantial than the flux decline at pH 3.0 (Figure 2a). These observations imply that charge neutralization has a more significant effect on foulant–foulant adhesion compared to charge screening and, hence, on the fouling behavior. Our observation is in agreement with previous studies suggesting that charge screening induced by increased indifferent salt

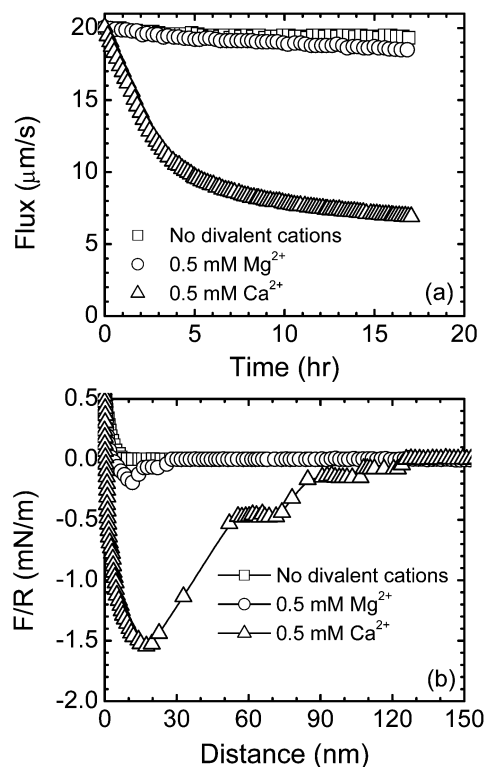


FIGURE 4. Effect of divalent cations on (a) flux decline during fouling and (b) intermolecular adhesion force. Both fouling runs and force measurements were performed with identical solutions (i.e., alginate = 20 mg/L, total ionic strength = 10 mM, and pH = 6.0 ± 0.1). The total ionic strength of the test solution is fixed at 10 mM by varying NaCl concentration (i.e., test solution with no divalent cations contains 10 mM NaCl and test solution with 0.5 mM Mg^{2+} or Ca^{2+} contains 8.5 mM NaCl). Other experimental conditions during the fouling runs and the force measurements were identical to those in Figure 2.

concentration does not significantly contribute to humic acid fouling (3, 4).

Influence of Divalent Cations. To investigate the influence of divalent calcium and magnesium ions on alginate fouling and intermolecular adhesion, fouling experiments and AFM measurements were performed in the presence of CaCl_2 and MgCl_2 . In these experiments, the total ionic strength was kept constant at 10 mM by adjusting the background NaCl concentration. Mg^{2+} and Ca^{2+} were chosen as model divalent cations because they are the major divalent cations in natural and waste waters. The permeate flux behavior during fouling and the corresponding measured adhesion force curves are presented in Figure 4.

As shown in Figure 4, the permeate flux declined precipitously during alginate fouling in the presence of Ca^{2+} , but not in the presence of Mg^{2+} . The flux decline in the presence of Mg^{2+} , however, was more substantial compared to that in the absence of divalent cations. Similarly, the adhesion force was quite significant (in magnitude and range) in the presence of Ca^{2+} , but much less in the presence of Mg^{2+} . No adhesion was observed in the absence of divalent cations (10 mM NaCl).

The effect of charge screening (or double layer compression) on reducing electrostatic repulsion among alginate molecules is expected to be similar in these cases because the total ionic strength was kept constant (3, 4). Therefore, the greater adhesion in the presence of divalent cations may be attributed to charge neutralization due to complexation of divalent cations to alginate carboxylic groups. Calcium ions have been shown to enhance NOM fouling by forming

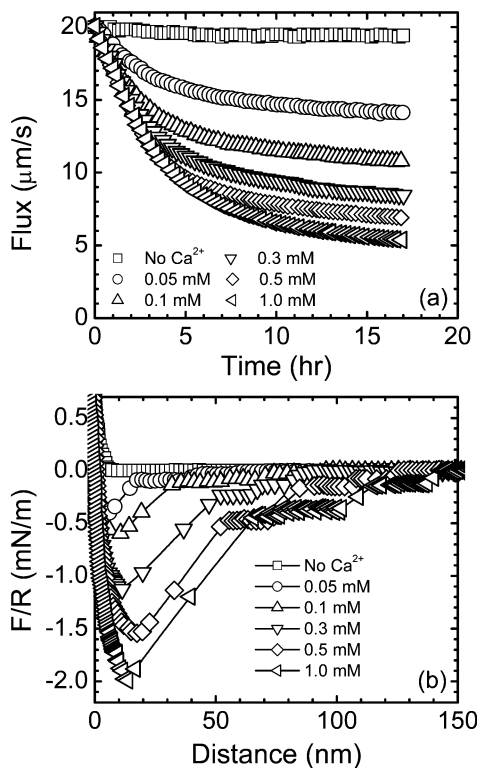


FIGURE 5. Effect of calcium concentration on (a) flux decline during fouling and (b) intermolecular adhesion force. Both fouling runs and force measurements were performed with identical solutions (i.e., alginate = 20 mg/L, total ionic strength = 10 mM, pH = 6.0 ± 0.1). The total ionic strength of the test solution is fixed at 10 mM by varying NaCl concentration (see caption of Figure 5). Other experimental conditions during the fouling runs and the force measurements were identical to those in Figure 2.

complexes with the carboxylic functional groups of NOM and neutralizing the negative charge of NOM molecules, leading to a thicker and more compact fouling layer (3, 4, 26).

There are several explanations for the vast difference in the adhesion force and the flux decline behavior in the presence of Ca²⁺ compared to Mg²⁺. Calcium ions are known to be more favorable divalent cations to form complexes with alginate molecules and, thus, should be more effective in charge neutralization (27, 28). However, the more effective charge neutralization by Ca²⁺ is not the major cause for the observed difference. The maximum adhesion force at pH 3.0 (-0.48 mN/m, Figure 2) was much less than that determined in the presence of Ca²⁺ (-1.62 mN/m, Figure 4). Complete charge neutralization takes place at pH 3.0 where the carboxylic groups of alginate molecules are protonated, yet the adhesion force is much lower than that with Ca²⁺. The remarkable adhesion force in the presence of calcium is attributed to intermolecular bridging between alginate molecules. This intermolecular bridging by calcium ions results in the formation of a cross-linked alginate gel layer on the membrane surface, which produces significant hydraulic resistance to permeate flow and, thus, a severe flux decline.

Alginate gel formation in the presence of calcium ions has been explained by the "egg-box" model (29). In this model, calcium ions bind preferentially to the carboxylic groups of alginate (and acidic polysaccharides) in a highly cooperative manner and form bridges between neighboring alginate molecules, leading to the egg-box-shaped gel network. Preferential calcium-alginate complexation and gel formation in the presence of Ca²⁺ has been reported

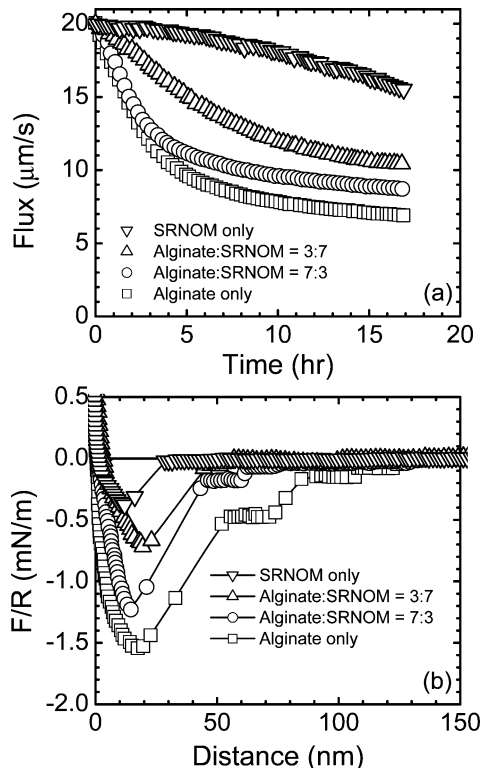


FIGURE 6. Effect of organic foulant composition of test solution on (a) flux decline during fouling and (b) intermolecular adhesion force. Both fouling runs and force measurements were performed with identical solutions (i.e., total organic concentration = 20 mg/L, calcium concentration = 0.5 mM, total ionic strength = 10 mM, and pH = 6.0 ± 0.1). The total organic foulant concentration of the test solution is fixed at 20 mg/L by varying the ratio of alginate to SRNOM concentration (i.e., test solution indicated as "Alginate only" contains 20 mg/L of alginate, test solution indicated as "Alginate:SRNOM = 7:3" contains 14 mg/L of alginate plus 6 mg/L of SRNOM, test solution indicated as "Alginate:SRNOM = 3:7" contains 6 mg/L of alginate plus 14 mg/L of SRNOM, and test solution indicated as "SRNOM only" contains 20 mg/L of SRNOM). Other experimental conditions during the fouling runs and the force measurements were identical to those in Figure 2.

elsewhere. Davis et al. (30) demonstrated enhanced selectivity of alginate molecules for calcium and cadmium relative to magnesium, leading to the formation of an alginate gel network. Bruus et al. (31) reported that the stability of biological flocs formed with alginate increased significantly in the presence of calcium ions as compared to magnesium ions, implying preferential alginate gel formation in the presence of calcium ions.

The influence of calcium ion concentration on alginate fouling and the corresponding intermolecular adhesion force was further investigated. Calcium concentration varied from 0.05 to 1.0 mM, keeping the total ionic strength constant at 10 mM. The results in Figure 5 clearly show that intermolecular adhesion forces increase substantially with increasing Ca²⁺ concentration. The results are attributed to enhanced intermolecular bridging between alginate molecules and accelerated gel formation. As gel formation increased with increasing calcium ion concentration, fouling became more severe as displayed by the permeate flux curves. It is interesting to note that the flux decline and the adhesion force curves at pH 3.0 presented earlier (Figure 2) are quite similar to those shown in Figure 5 for 0.05 mM Ca²⁺. This implies that 0.05 mM calcium is not enough to form intermolecular bridging between alginate molecules. Thus, the stoichiometry between calcium and alginate concentra-

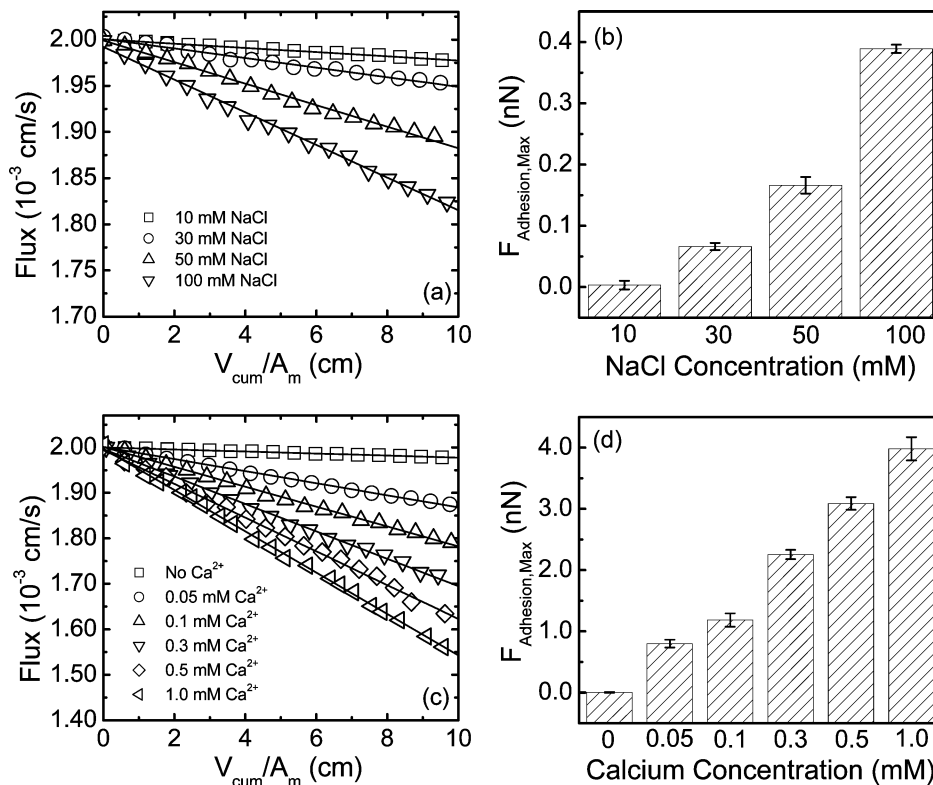


FIGURE 7. Relating fouling rate to the maximum adhesion force: (a) flux decline with respect to cumulative permeate volume (V_{cum}) per unit membrane area (A_m) at different NaCl concentrations, (b) maximum adhesion force ($F_{ad,max}$) with respect to NaCl concentrations (error bars indicate one standard deviation), (c) flux decline with respect to V_{cum}/A_m at different calcium concentrations, and (d) $F_{ad,max}$ with respect to calcium concentrations (error bars indicate one standard deviation). The solid lines included in Figures 7a and c were produced by a linear fitting of the flux versus V_{cum}/A_m data. Fouling rate was determined from the slope of each solid line. Flux–decline data were adopted from the results shown in Figures 3a and 5a, and the maximum adhesion force was determined from the results shown in Figures 3b and 5b.

tions is also expected to play an important role in the formation of an alginate gel network.

A characteristic feature of the adhesion force curves in the presence of Ca $^{2+}$ (Figures 4b and 5b) is the very long range of adhesion compared to Mg $^{2+}$ (Figure 4b), Na $^{+}$ (Figure 3b), and pH variations (Figure 2b). For instance, at 1 mM Ca $^{2+}$ (Figure 5b), the adhesion force reached up to a separation distance of 150 nm. We propose that this long-range adhesion confirms the intermolecular bridging between alginate macromolecules in the presence of Ca $^{2+}$. Intermolecular bridging allows the stretching of the alginate macromolecules in the gel network upon retraction of the AFM foulant probe from the membrane surface until a complete detachment takes place. In addition, there exist several plateaus in the adhesion force profiles at high calcium concentrations. This implies that a complete detachment of the AFM foulant probe from the membrane surface is accomplished by the sequential detachment of all bridged macromolecules between the probe and the fouled membrane. These observations suggest that AFM force measurements allow not only the quantitative measurement of the adhesion force but also qualitative understanding of the foulant–foulant interaction.

Influence of Organic Foulant Composition. Fouling experiments and force measurements were performed with test solutions containing different mass ratios of alginate to SRNOM. Four foulant compositions were examined with the total foulant concentration being maintained at 20 mg/L: 20 mg/L alginate and no SRNOM, 14 mg/L alginate plus 6 mg/L SRNOM (alginate to SRNOM mass ratio of 7:3), 6 mg/L alginate plus 14 mg/L SRNOM (alginate to SRNOM mass ratio of 3:7), and 20 mg/L SRNOM and no alginate. The permeate flux decline during fouling and the corresponding

adhesion forces for these foulant combinations are presented in Figure 6.

The intermolecular adhesion in the presence of Ca $^{2+}$ was much greater for alginate (and no SRNOM) than for SRNOM (and no alginate), with corresponding maximum adhesion forces of -1.62 mN/m and -0.49 mN/m, respectively. Accordingly, the permeate flux decline for alginate fouling was more substantial compared to SRNOM fouling. When the test solutions contained both alginate and SRNOM, the adhesion force and flux decline were more substantial for higher alginate concentrations. We propose this behavior is attributed to structural differences between alginate and SRNOM molecules along with the resulting fouling layer structure.

The significant differences in the fouling and adhesion force curves for alginate and SRNOM cannot be attributed to lack of interaction between calcium ions and SRNOM. Humic molecules can form a cross-linked fouling layer in the presence of Ca $^{2+}$ via calcium binding with humic carboxylic groups and bridging among adjacent humic molecules (3). As shown earlier, the humic content of the SRNOM was more than 70%, and carboxylic groups were the predominant functional groups of SRNOM. We attribute the much greater observed adhesion force with alginate than SRNOM to the gel-forming nature of alginate, where intermolecular adhesion needs to be strong enough to sustain the structural integrity of the gel network. It has been reported that gelation of charged macromolecules by intermolecular bridging is predominant for hydrophilic organic macromolecules (such as acidic polysaccharides) compared to hydrophobic organic macromolecules (such as humic acids) (29, 32, 33). In addition to the greater intermolecular adhesion of the alginate gel network, the larger size of alginate

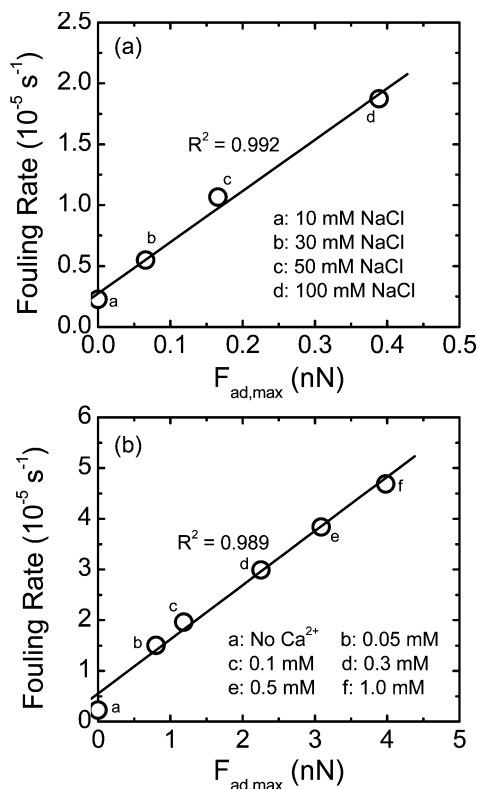


FIGURE 8. Correlation between the fouling rate and the maximum adhesion force with respect to (a) NaCl concentration and (b) calcium concentration.

compared to SRNOM may also be responsible for the formation of a thicker fouling layer on the membrane surface and, thus, more severe flux decline during fouling.

Correlation between Fouling and Intermolecular Adhesion Force. The results presented earlier in this paper suggest that organic fouling behavior is related to the measured intermolecular adhesion force. Here, we correlate the fouling rate determined from the flux–decline curves to the corresponding maximum adhesion force. Fouling rate was determined from the slope of the linear region of the flux–decline curve with respect to the cumulative permeate volume (V_{cum}) per unit membrane surface area (A_m) (34). The linear flux decline with respect to V_{cum}/A_m represents a constant increase in the hydraulic resistance of the fouling layer due to the steady evolution of the fouling layer, which is governed by foulant–foulant interaction. Foulant adhesion, represented by the maximum adhesion force ($F_{ad,max}$), was directly obtained from the force versus separation distance curves shown previously. The initial fouling rate curves and the maximum adhesion forces determined at different ionic strengths and calcium concentrations are presented in Figure 7; the corresponding correlations between the fouling rate and the adhesion force are shown in Figure 8.

A striking correlation between the fouling rate and the maximum adhesion force is displayed for the runs with NaCl and $CaCl_2$. This direct relationship between organic fouling and intermolecular adhesion confirms our previous finding that foulant–foulant interaction plays a key role in determining the rate and extent of organic fouling (3). In our earlier analysis, F_{ad}/R (eq 2) was defined as the measure of the energy required to prevent a foulant from accumulating on the membrane surface. The strong correlation between F_{ad} and fouling rate depicted in Figure 8 supports our suggestion that the foulant adhesion force can serve as an indicator of fouling potential.

Intermolecular adhesion can also be quantified by integrating the adhesion force as a function of distance for each solution condition employed. The integrated area of the adhesion curve is indicative of the total adhesion energy between foulants. Carrying out such a procedure for the force data displayed in Figures 3b and 5b (data not shown) revealed a similarly remarkable correlation between the fouling rate and the obtained interaction energies, with graphs quite similar to those displayed in Figure 8. The R^2 values for the runs with NaCl and $CaCl_2$ were 0.972 and 0.933, respectively. These values are very close to those obtained in Figure 8.

Acknowledgments

This study was supported by the U.S. Department of Interior, Bureau of Reclamation, Desalination and Water Purification Research and Development Program.

Literature Cited

- Jarusutthirak, C.; Amy, G.; Croué, J.-P. Fouling characteristics of wastewater effluent organic matter (EfOM) isolates on NF and UF membranes. *Desalination* **2002**, *145*, 247.
- Into, M.; Jönsson, A.-S.; Lengdén, G. Reuse of industrial wastewater following treatment with reverse osmosis. *J. Membr. Sci.* **2004**, *242*, 21.
- Li, Q.; Elimelech, M. Organic fouling and chemical cleaning of nanofiltration membranes: Measurements and mechanisms. *Environ. Sci. Technol.* **2004**, *38*, 4683.
- Hong, S.; Elimelech, M. Chemical and physical aspects of natural organic matter (NOM) fouling of nanofiltration membranes. *J. Membr. Sci.* **1997**, *132*, 159.
- Ducker, W. A.; Senden, T. J.; Pashley, R. M. Direct measurement of colloidal forces using an atomic force microscope. *Nature* **1991**, *353*, 239.
- Butt, H.-J.; Jaschke, M.; Ducker, W. Measuring surface forces in aqueous electrolyte solution with the atomic force microscope. *Bioelectrochem. Bioenerg.* **1995**, *38*, 191.
- Hilal, N.; Kochkodan, V. Surface modified microfiltration membranes with molecularly recognizing properties. *J. Membr. Sci.* **2003**, *213*, 97.
- Hilal, N.; Busca, G.; Talens-Alesson, F.; Atkin, B. P. Treatment of waste coolants by coagulation and membrane filtration. *Chem. Eng. Process.* **2004**, *43*, 811.
- Hilal, N.; Al-Zoubi, H.; Darwish, N. A.; Mohammad, A. W.; Arabi, M. A. A comprehensive review of nanofiltration membranes: Treatment, pretreatment, modeling, and atomic force microscopy. *Desalination* **2004**, *170*, 281.
- Manka, J.; Rebhun, M.; Mandelbaum, A.; Borginger, A. Characterization of organics in secondary effluents. *Environ. Sci. Technol.* **1974**, *8*, 1017.
- Barker, D. J.; Stuckey, D. C. A review of soluble microbial products (SMP) in wastewater treatment systems. *Water Res.* **1999**, *33*, 3063.
- Barker, D. J.; Salvi, S. M. L.; Langenhoff, A. A. M.; Stuckey, D. C. Soluble Microbial Products in ABR Treating Low-Strength Wastewater. *J. Environ. Eng.* **2000**, *126*, 239.
- Aiken, G. R.; McKnight, D. M.; Thorn, K. A. Isolation of hydrophilic organic acids from water using nonionic macroporous resins. *Org. Geochem.* **1992**, *18*, 567.
- Lee, S.; Amy, G.; Cho, J. Applicability of Sherwood correlations for natural organic matter (NOM) transport in nanofiltration (NF) membranes. *J. Membr. Sci.* **2004**, *240*, 49.
- Draget, K. I.; Skjåk Bræk, G.; Smidsrød, O. Alginic acid gels: the effect of alginate chemical composition and molecular weight. *Carbohydr. Polym.* **1994**, *25*, 31.
- Aleixo, L. M.; Godinho, O. S. E.; da Costa, W. F. Potentiometric study of acid–base properties of humic acid using linear functions for treatment of titration data. *Anal. Chim. Acta* **1992**, *257*, 35.
- Vrijenhoek, E. M.; Hong, S.; Elimelech, M. Influence of membrane surface properties on initial rate of colloidal fouling of reverse osmosis and nanofiltration membranes. *J. Membr. Sci.* **2001**, *188*, 115.
- Ang, W. S.; Lee, S.; Elimelech, M. Chemical and physical aspects of cleaning of organic-fouled reverse osmosis membranes. *J. Membr. Sci.* (doi: 10.1016/j.memsci.2005.07.035).

- (19) Florin, E. L.; Moy, V. T.; Gaub, H. E. Adhesion forces between individual ligand–receptor pairs. *Science* **1994**, *264*, 415.
- (20) Ducker, W. A.; Senden, T. J.; Pashley, R. M. Measurement of forces in liquids using a force microscope. *Langmuir* **1992**, *8*, 1831.
- (21) Israelachvili, J. N. *Intermolecular and Surface Forces*, 2nd ed.; Academic Press: New York, 1992.
- (22) Thurman, E.; Malcolm, R. Preparative isolation of aquatic humic substances. *Environ. Sci. Technol.* **1981**, *15*, 463.
- (23) Collins, M. R.; Amy, G.; Steelink, C. Molecular weight distribution, carboxylic acidity, and humic substances content of aquatic organic matter: Implication for removal during water treatment. *Environ. Sci. Technol.* **1986**, *20*, 1028.
- (24) Braghetta, A.; DiGiano, F. A.; Ball, W. P. Nanofiltration of natural organic matter: pH and ionic strength effects. *J. Environ. Eng. ASCE* **1997**, *123*, 628.
- (25) Chan, R.; Chen, V. The effects of electrolyte concentration and pH on protein aggregation and deposition: critical flux and constant flux membrane filtration. *J. Membr. Sci.* **2001**, *185*, 177.
- (26) Lee, S.; Cho, J.; Elimelech, M. A novel method for investigating the influence of feed water recovery on colloidal and NOM fouling of RO and NF membranes. *Environ. Eng. Sci.* **2005**, *22*, 496.
- (27) Davis, T. A.; Voleskey, B.; Mucci, A. A review of the biochemistry of heavy metal biosorption by brown algae. *Water Res.* **2003**, *37*, 4311.
- (28) Lattner, D.; Flemming, H.-C.; Mayer, C. ¹³C NMR study of the interaction of bacterial alginate with bivalent cations. *Int. J. Biol. Macromol.* **2003**, *33*, 81.
- (29) Grant, G. T.; Morris, E. R.; Rees, D. A.; Smith, J. C.; Thom, D. Biological interaction between polysaccharides and divalent cations: egg-box model. *FEBS Lett.* **1973**, *32*, 195.
- (30) Davis, T. A.; Llanes, F.; Voleskey, B.; Mucci, A. Metal selectivity of *Sargassum* spp. and their alginates in relation to their α-L-guluronic acid content and conformation. *Environ. Sci. Technol.* **2003**, *37*, 261.
- (31) Bruus, J. H.; Nielsen, P. H.; Keiding, K. On the stability of activated sludge flocs with implications to dewatering. *Water Res.* **1992**, *26*, 1597.
- (32) Decho, A. W. Imaging an alginate polymer gel matrix using atomic force microscopy. *Carbohydr. Res.* **1999**, *315*, 330.
- (33) Donati, I.; Coslovi, A.; Gamini, A.; Skjåk-Bræk, G.; Vetere, A.; Campa, C.; Paoletti, S. Galactose-Substituted Alginate 2: Conformational Aspects. *Biomacromolecules* **2004**, *5*, 186.
- (34) Song, L.; Chen, K. L.; Ong, S. L.; Ng, W. J. A new normalization method for determination of colloidal fouling potential in membrane processes. *J. Colloid Interface Sci.* **2004**, *271*, 426.

Received for review September 15, 2005. Revised manuscript received November 16, 2005. Accepted November 25, 2005.

ES051825H